Do nuclei assume toroidal shapes?

A. Staszczak, C. Y. Wong, A. Kosior

„PRZYSZŁOŚĆ FIZYKI JĄDROWEJ NISKICH ENERGII W POLSCE
A ROZWÓJ KRAJOWEJ INFRASTRUKTURY BADAWCZEJ"
14-15 stycznia 2019 r.
Środowiskowe Laboratorium Ciężkich Jonów UW

The equality-constrained problem (ECP) in nuclear density functional theory (DFT)

$$\begin{cases} \min_{\bar{\rho}} E^{tot}[\bar{\boldsymbol{\rho}}] \\ \text{subject to:} \quad \sum_{q=p,n} \langle \Phi(\bar{\boldsymbol{\rho}}) | \hat{N}_q | \Phi(\bar{\boldsymbol{\rho}}) \rangle = N_q, \\ \qquad\qquad\qquad \sum_{\lambda\mu} \langle \Phi(\bar{\boldsymbol{\rho}}) | \hat{Q}_{\lambda\mu} | \Phi(\bar{\boldsymbol{\rho}}) \rangle = Q_{\lambda\mu}, \end{cases}$$

$$\begin{aligned} E^{tot}[\bar{\boldsymbol{\rho}}] &\equiv E^{tot}\left[\rho, \tau, \mathbb{J}; \boldsymbol{s}, \boldsymbol{T}, \boldsymbol{j}, \boldsymbol{F}; \tilde{\rho}\right] \\ &= \int \mathrm{d}^3\boldsymbol{r} \left(\mathcal{E}_{kin}(\boldsymbol{r}) + \mathcal{E}_{Sk}(\boldsymbol{r}) + \mathcal{E}^{dir}_{Coul}(\boldsymbol{r}) + \mathcal{E}^{ex}_{Coul}(\boldsymbol{r}) + \mathcal{E}_{pair}(\boldsymbol{r})\right) + E_{corr} \end{aligned}$$

an objective function

The Skyrme EDF in the case of even-even nuclei (time-reversal symmetry)

$$\begin{aligned} \mathcal{E}^{even}_{Sk}(\boldsymbol{r}) &= \sum_{t=0,1} \left(C^{\rho}_t[\rho_0]\rho_t^2 + C^{\Delta\rho}_t \rho_t \Delta\rho_t + C^{\tau}_t \rho_t \tau_t + C^{J}_t \mathbb{J}^2_t \right) \quad \text{(central terms)} \\ &+ \sum_{t=0,1} \left(C^{\nabla J}_t \rho_t \boldsymbol{\nabla} \cdot \boldsymbol{J}_t \right), \quad \text{(spin-orbit term)} \end{aligned}$$

The total energy in the Skyrme-HF/HFB model

$$E^{tot} \equiv \langle \Phi_{HF}|\hat{H}|\Phi_{HF}\rangle \geqslant E_{g.s.}$$
$$= \int \mathrm{d}^3\boldsymbol{r}\ \left[\mathcal{E}_{kin} + \mathcal{E}_{Sk} + \mathcal{E}_{Coul}^{dir} + \mathcal{E}_{Coul}^{ex} + \mathcal{E}_{pair}\right] + E_{corr},$$

$$\mathcal{E}_{kin} = \frac{\hbar^2}{2m}\tau_0(\boldsymbol{r}),$$ kinetic energy density

$$\mathcal{E}_{Coul}^{dir} = \tfrac{1}{2}e^2\rho_p(\boldsymbol{r})\int \mathrm{d}^3\boldsymbol{r}'\ \frac{\rho_p(\boldsymbol{r}')}{|\ \boldsymbol{r}-\boldsymbol{r}'\ |},$$ direct Coulomb en. density

$$\mathcal{E}_{Coul}^{ex} = -\tfrac{3}{4}e^2\left(\tfrac{3}{\pi}\right)^{1/3}\rho_p^{4/3}(\boldsymbol{r})$$ exchange Coulomb en. density (in the Slater approx.)

$$\mathcal{E}_{pair} = \sum_{q=p,n}\frac{V_q^0}{4}\left[1 - V^1\left(\frac{\rho_0(\boldsymbol{r})}{\rho_{st}}\right)^{\beta}\right]\tilde{\rho}_q^2(\boldsymbol{r}),$$ isovector pairing en. density

$V^1 = 0,\ 1,\ \text{or}\ 1/2$ for *volume-*, *surface-*, or *mix-*type pairing

$\rho_{st} = 0.16\ \mathrm{fm}^{-3}$

HFODD: the self-consistent symmetries

- time-reversal $\hat{T}$
- parity $\hat{P}$
- x-, y-, z-signature $\hat{R}_{x,y,z} = \exp(-i\pi \hat{J}_{x,y,z})$
- x-, y-, z-simplex $\hat{S}_{x,y,z} = \hat{P}\hat{R}_{x,y,z}$
- x-, y-, z-simplex*T $\hat{S}^T_{x,y,z} = \hat{T}\hat{S}_{x,y,z}$

$\hat{T}$	$\hat{S}_y$	$\hat{S}^T_y$
$\hat{P}$	$\hat{S}_y$	$\hat{R}_y$
$\hat{R}_y$	$\hat{S}^T_x$	$\hat{S}^T_z$
1	1	1
1	0	0
0	1	0
0	0	1
0	0	0

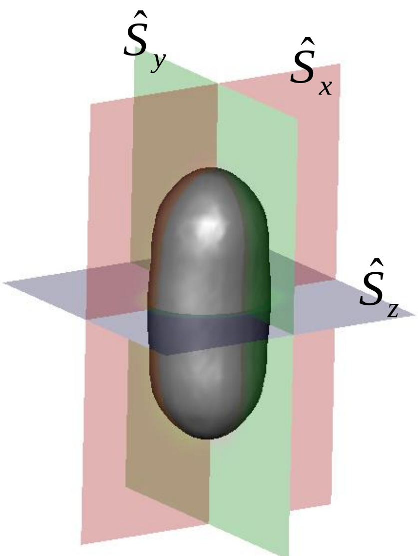

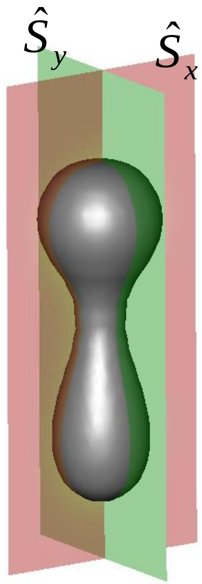

$$\hat{S}_y = 1 \Rightarrow Q_{\lambda\mu} = \langle \hat{Q}_{\lambda\mu} \rangle \in \mathbb{R}$$

$$Q_{\lambda-\mathrm{odd},\mu} \neq 0 \;\; only \;\; for \;\; \hat{P} = 0$$

Examination of evidence for resonances at high excitation energy in the 7α disassembly of ^{28}Si

X. G. Cao,[1,2,3,4] E. J. Kim,[2,5] K. Schmidt,[6,2] K. Hagel,[2] M. Barbui,[2] J. Gauthier,[2] S. Wuenschel,[2] G. Giuliani,[2,7] M. R. D. Rodriguez,[2,8] S. Kowalski,[6] H. Zheng,[2,9] M. Huang,[2,10] A. Bonasera,[2,7] R. Wada,[2] N. Blando,[2] G. Q. Zhang,[1,2] C. Y. Wong,[11] A. Staszczak,[12] Z. X. Ren,[13] Y. K. Wang,[13] S. Q. Zhang,[13] J. Meng,[13,14] and J. B. Natowitz[2]
[1]*Shanghai Institute of Applied Physics, Chinese Academy of Sciences, Shanghai 201800, China*
[2]*Cyclotron Institute, Texas A&M University, College Station, Texas 77843, USA*
[3]*Shanghai Advanced Research Institute, Chinese Academy of Sciences, Shanghai 201210, China*
[4]*Zhangjiang Laboratory, Shanghai 201210, China*
[5]*Division of Science Education, Chonbuk National University, 567 Baekje-daero Deokjin-gu, Jeonju 54896, Korea*
[6]*Institute of Physics, University of Silesia, 40-007 Katowice, Poland*
[7]*Laboratori Nazionali del Sud, Istituto Nazionale di Fisica Nucleare (INFN), via Santa Sofia, 62, 95123 Catania, Italy*
[8]*Instituto de Física, Universidade de São Paulo, Caixa Postal 66318, CEP 05389-970, São Paulo, São Paulo, Brazil*
[9]*School of Physics and Information Technology, Shaaxi Normal University, Xi'an 710119, China*
[10]*College of Physics and Electronics Information, Inner Mongolia University for Nationalities, Tongliao, 028000, China*
[11]*Physics Division, Oak Ridge National Laboratory, Oak Ridge, Tennessee, USA*
[12]*Institute of Physics, Maria Curie-Skłodowska University, Lublin, Poland*
[13]*State Key Laboratory of Nuclear Physics and Technology, School of Physics, Peking University, Beijing 100871, China*
[14]*Yukawa Institute for Theoretical Physics, Kyoto University, Kyoto 606-8502, Japan*

(Received 18 July 2018; revised manuscript received 22 October 2018; published 7 January 2019)

The experimental excitation function for the 7α de-excitation of ^{28}Si nuclei excited to high excitation energies in the collisions of 35 MeV/nucleon ^{28}Si with ^{12}C reveals resonance structures. The possibility that these structures may indicate the population of toroidal high-spin isomers such as those predicted by a number of recent theoretical calculations is discussed and the need for further investigations is emphasized.

DOI: 10.1103/PhysRevC.99.014606

Here we report results for an investigation of ^{28}Si, focusing on the 7α decay channels of excited projectile-like fragments produced in the reaction 35 MeV/nucleon ^{28}Si + ^{12}C. In this reaction the energy available in the center of mass is 294 MeV. Interpolation of the systematic calculations of the authors of [44] indicate that the maximum angular momentum, $L_{\max}$, is 94$\hbar$ (a reaction cross section of 2417 mb), L_{crit} for fusion is 26$\hbar$ and the rotating liquid drop limiting angular momentum is 40$\hbar$. These parameters indicate that the bulk of the reaction cross section will lead, not to fusion, but to initially binary configurations of excited projectile-like and target-like nuclei.

Motivated by the predictions of toroidal isomeric states in a number of light nuclei, we have undertaken searches for evidence of their existence. For ^{28}Si, the nucleus investigated in the present work, the Staszczak and Wong calculations indicate that toroidal shapes with $I = 0$ become possible at excitation energies greater than 85 MeV. The existence of a stabilized state with angular momentum of 44$\hbar$ and excitation energy of 143.18 MeV [16] was predicted. See Table I.

TABLE I. Calculated parameters for the predicted toroidal isomer in ^{28}Si. Left to right: Spin $I = I_z$, quadrupole moment Q_{20}, the cranking rotation frequency $\hbar\omega$, excitation energy E_x, toroidal major radius R, minor radius d, aspect ratio R/d, and maximum density $\rho_{\max}$

	I [$\hbar$]	Q_{20} [b]	$\hbar\omega$ [MeV]	E_x [MeV]	R [fm]	d [fm]	R/d	$\rho_{\max}$ [fm^{-3}]
^{28}Si	44	−5.86	2.8	143.18	4.33	1.45	2.99	0.119

[16] A. S. and C. Y. Wong, *A region of high-spin toroidal isomers*, Phys. Lett. B **738**, 401 (2014).

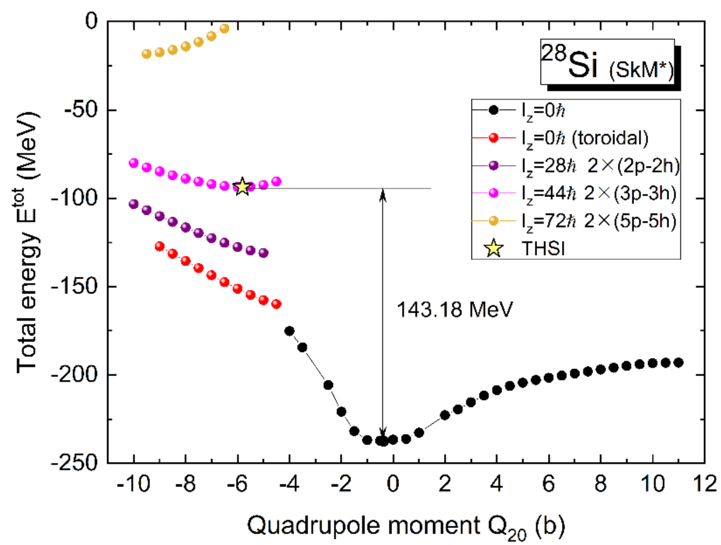

The experiment was performed at Texas A&M University Cyclotron Institute. A 35 MeV/nucleon ^{28}Si beam produced by the *K*500 superconducting cyclotron impinged on a ^{12}C target. The reaction products were measured using a 4π array Neutron Ion Multidetector for Reaction Oriented Dynamics with the Indiana Silicon Sphere (NIMROD-ISiS) [45,46], which consisted of 14 concentric rings covering from 3.6° to 167° in the laboratory frame [45]. In the forward rings

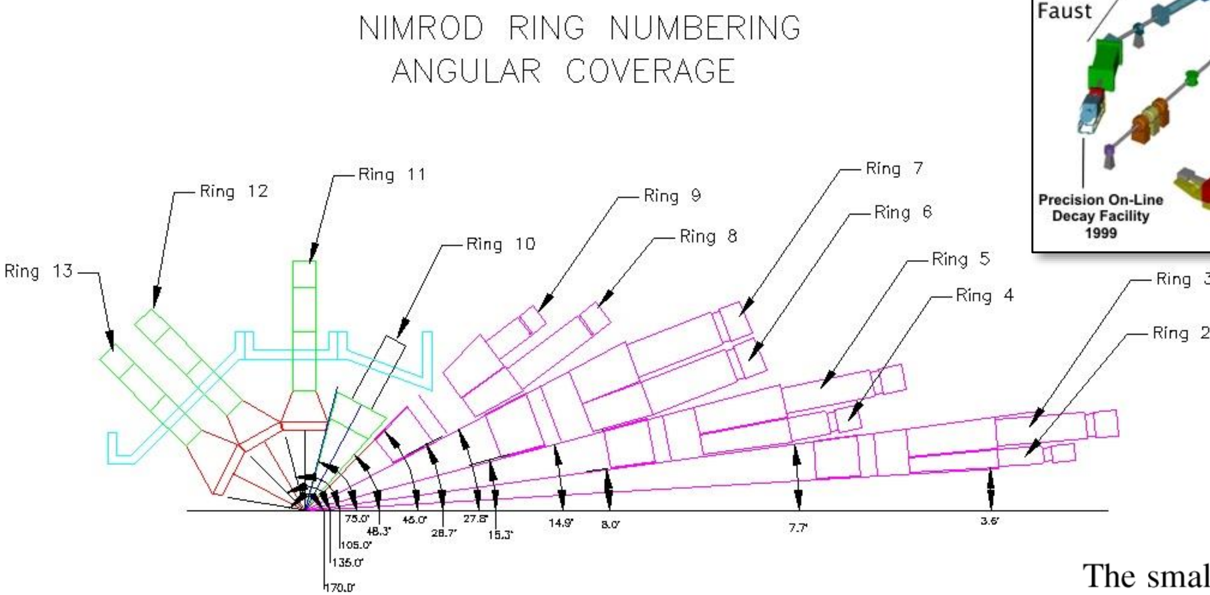

For the ^{28}Si + ^{12}C reaction, a total of 17.5 million events were recorded and a significant proportion of events had significant α-like (AL) mass emission (i.e., α-particles or α-conjugate nuclei). About 3.19×10^5 events had AL = 28. Of these 6467 detected events had seven α-particles.

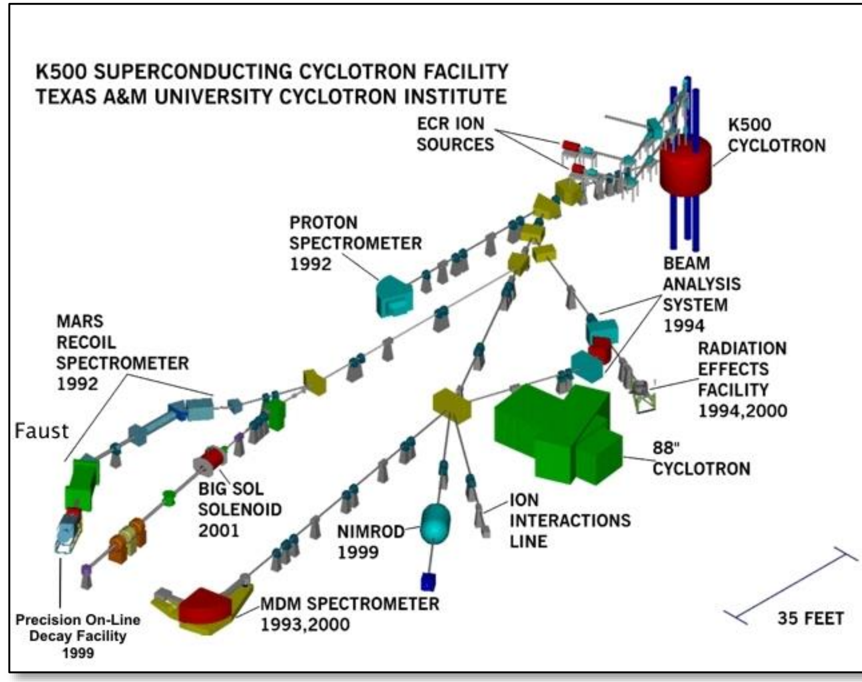

The smallest energy of detected α-particle in 7α events is about 3.3 MeV in the laboratory frame. Thresholds are similar for other α-conjugate exit channels. Using the AMD + GEMINI simulation analysis before and after experimental filtering, we estimate the detection efficiency for 7α events to be 0.108. The detected event numbers of 6α, 7α, and 8α events are 24 849, 6467, and 840, respectively. The ratio between them is 1:0.26:0.03.

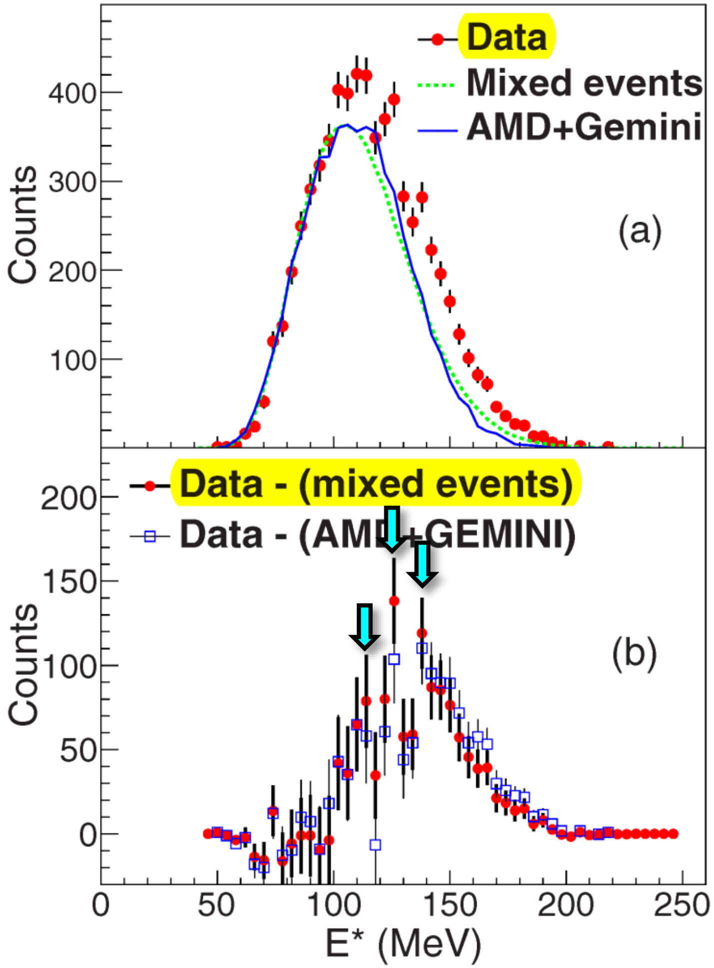

FIG. 2. Excitation energy distribution leading to observed 7α events. Top Panel: The data are represented by solid red circles. An uncorrelated spectrum derived from event mixing is represented by the dotted green line. The filtered result from an AMD-GEMINI calculation is indicated by the solid blue line (see text). The last two are normalized to the experimental spectrum at the lower edge of the spectrum. Bottom Panel: The differences between the experimental spectrum and the others are presented. Relative to the uncorrelated background derived from the experiment the statistical significance of the difference peak at 114 MeV is 5.0σ, at 126 MeV is 7.9σ, and at 138 MeV is 7.1σ. See text.

In Fig. 2(a), we compare the experimental spectrum for the 7α events to an uncorrelated 7α spectrum. The spectrum of uncorrelated events was constructed by randomly selecting seven α-particles from seven different events. The random selection was done many times to assure that the statistical fluctuations for this spectrum would be much lower than those of the correlated event spectrum. This uncorrelated spectrum

COMPARISON TO TOROIDAL SHELL MODEL

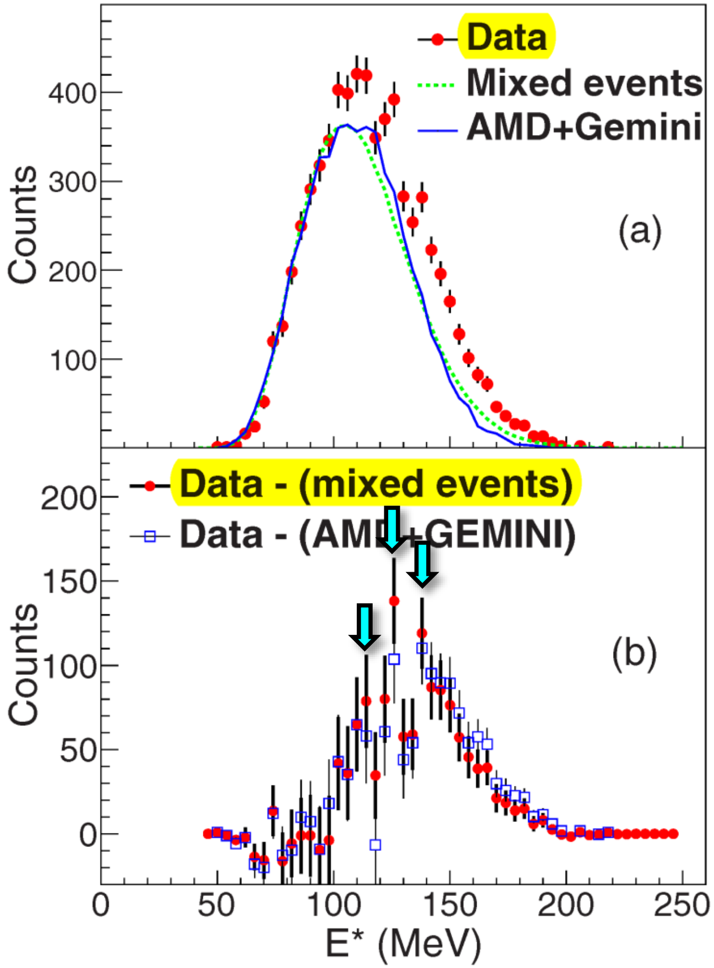

FIG. 2. Excitation energy distribution leading to observed 7α events. Top Panel: The data are represented by solid red circles. An uncorrelated spectrum derived from event mixing is represented by the dotted green line. The filtered result from an AMD-GEMINI calculation is indicated by the solid blue line (see text). The last two are normalized to the experimental spectrum at the lower edge of the spectrum. Bottom Panel: The differences between the experimental spectrum and the others are presented. Relative to the uncorrelated background derived from the experiment the statistical significance of the difference peak at 114 MeV is 5.0σ, at 126 MeV is 7.9σ, and at 138 MeV is 7.1σ. See text.

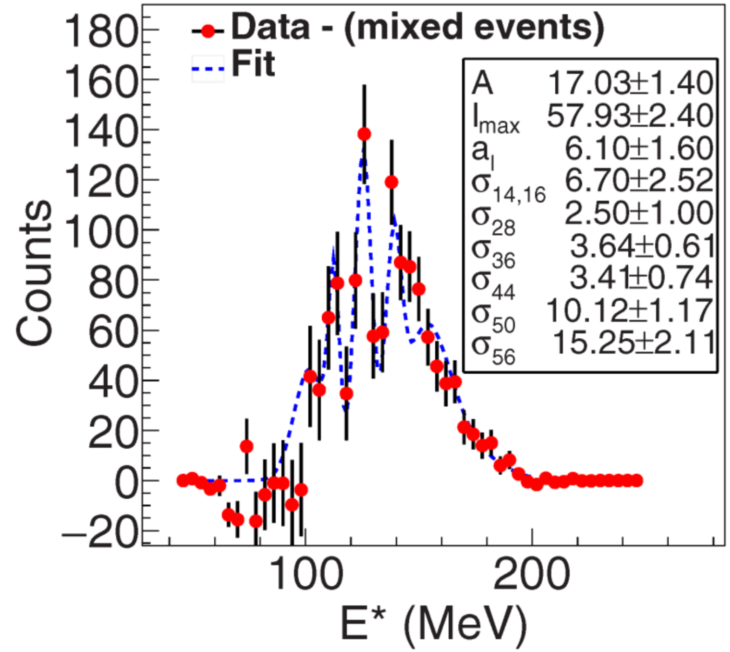

FIG. 4. The experimental (correlated data)–(mixed event data) (solid points) are compared to the results of semi-empirical formula (4) containing the signature of the toroidal high-spin isomers as primary ingredients (dashed curve) with the list of extracted widths and other parameters.

$$\sigma_{\text{toroidal}}(E_x, 7\alpha) = A \sum_{I=I_{\text{toroid}}} \frac{g_I I}{1+\exp\{(I-I_{\max})/a\}} \times \frac{1}{\sqrt{2\pi}\sigma_I} \exp\{-(E_x - E_I)^2/2\sigma_I^2\}, \quad (4)$$

Configurations	I	$(E_I - E_0)$ in $\hbar^2/2mR^2$	E_I (MeV)
$(0p\text{-}0h)_\nu(0p\text{-}0h)_\pi$	0	0	91.82
$(1p\text{-}1h)_\nu(1p\text{-}1h)_\pi$	16	14	101.2
$(0p\text{-}0h)_\nu(2p\text{-}2h)_\pi+(2p\text{-}2h)_\nu(0p\text{-}0h)_\pi$	14	14	101.2
$(2p\text{-}2h)_\nu(2p\text{-}2h)_\pi$	28	28	110.58
$(2p\text{-}2h)_\nu(3p\text{-}3h)_\pi+(3p\text{-}3h)_\nu(2p\text{-}2h)_\pi$	36	49	124.65
$(3p\text{-}3h)_\nu(3p\text{-}3h)_\pi$	44	70	138.72
$(3p\text{-}3h)_\nu(4p\text{-}4h)_\pi+(4p\text{-}4h)_\nu(3p\text{-}3h)_\pi$	50	91	152.79
$(4p\text{-}4h)_\nu(4p\text{-}4h)_\pi$	56	112	166.86

Light N=Z toroidal nuclei in constrained SkM*-HFB model

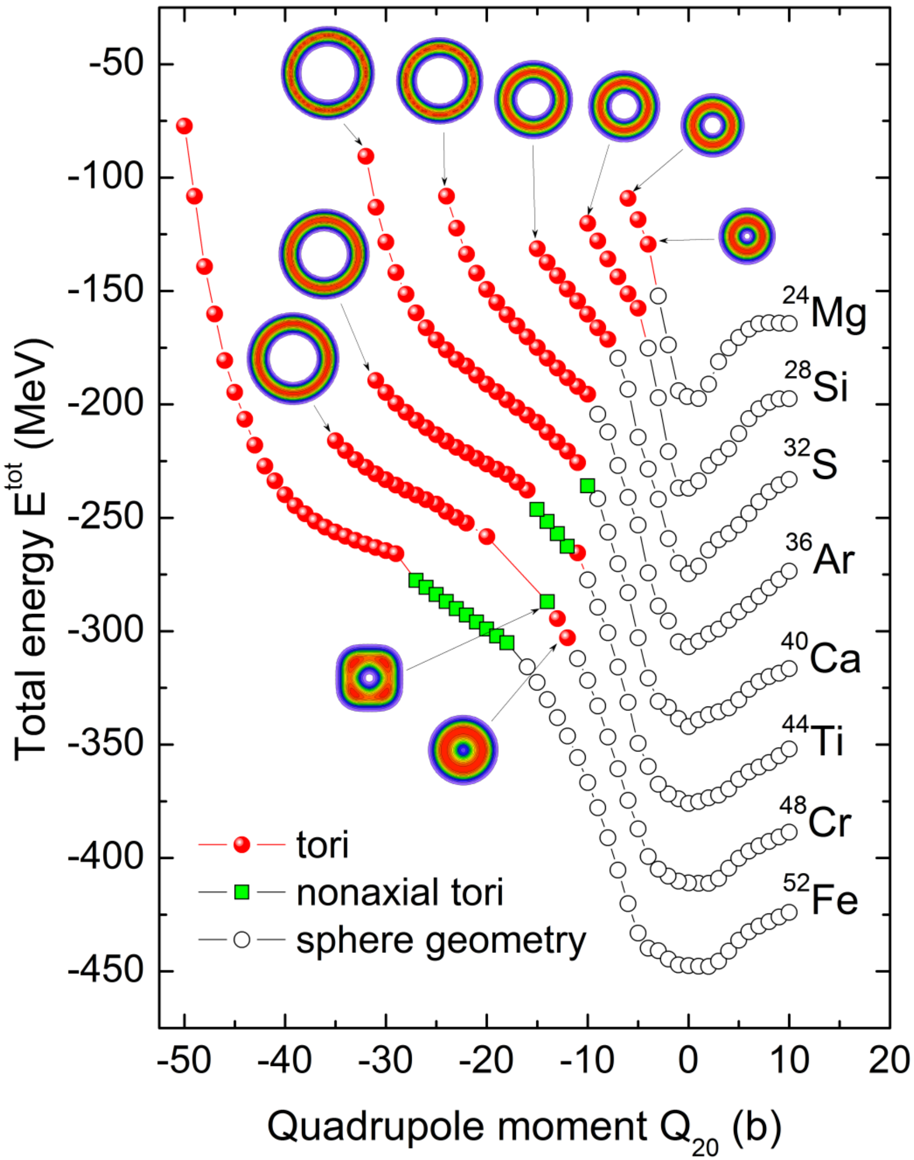

Toroidal nuclei in cranked SkM*-HF model

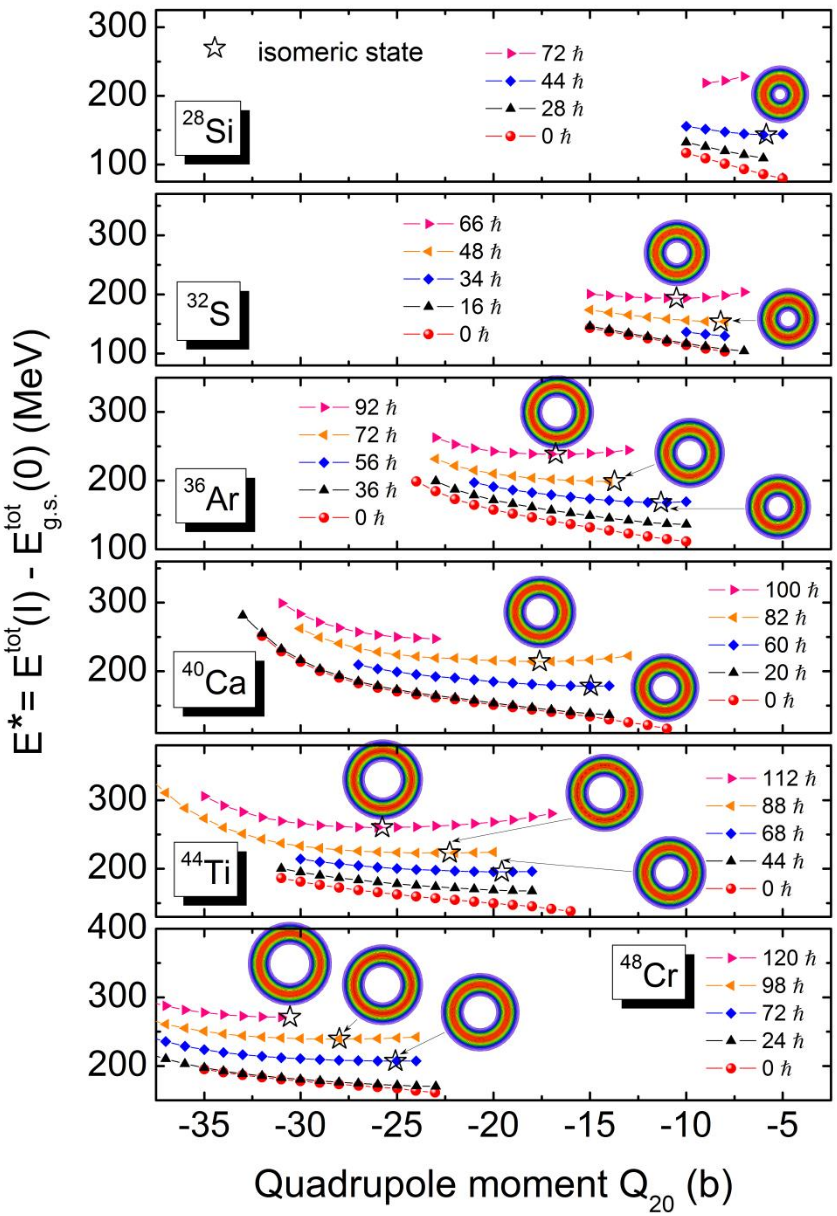

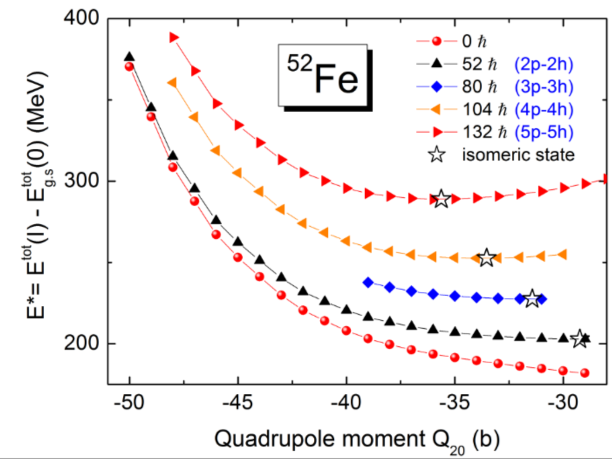

Table 1
Properties of high-spin toroidal isomers at their local energy minima in $28 \leqslant A \leqslant 52$.

	$I/\hbar$	Q_{20} (b)	$\hbar\omega$ (MeV)	E^* (MeV)	R (fm)	d (fm)	R/d	ρ_{max} (fm^{-3})
^{28}Si	44	−5.86	2.8	143.18	4.33	1.45	2.99	0.119
^{32}S	48	−8.22	1.9	153.87	4.87	1.42	3.43	0.122
	66	−10.51	2.2	193.35	5.57	1.40	3.98	0.108
^{36}Ar	56	−11.31	1.7	168.03	5.44	1.40	3.88	0.125
	72	−13.73	1.85	198.63	6.04	1.39	4.34	0.113
	92	−16.78	2.0	238.56	6.73	1.37	4.91	0.103
^{40}Ca	60	−14.96	1.5	178.36	5.97	1.40	4.26	0.126
	82	−17.61	1.9	214.23	6.51	1.39	4.68	0.117
^{44}Ti	68	−19.57	1.2	195.46	6.55	1.39	4.71	0.128
	88	−22.27	1.4	223.09	7.01	1.38	5.08	0.120
	112	−25.76	1.6	260.24	7.56	1.37	5.52	0.113
^{48}Cr	72	−25.08	1.2	207.12	7.12	1.38	5.16	0.128
	98	−28.00	1.4	239.26	7.54	1.37	5.50	0.122
	120	−30.55	1.43	271.02	7.90	1.36	5.81	0.118
^{52}Fe	52	−29.24	0.8	202.86	7.39	1.38	5.35	0.134
	80	−31.43	0.95	227.54	7.68	1.38	5.56	0.130
	104	−33.54	1.3	252.65	7.94	1.37	5.79	0.126
	132	−35.62	1.5	288.91	8.20	1.36	6.03	0.123

A. S. and C. Y. Wong, *A region of high-spin toroidal isomers*, Phys. Lett. B **738**, 401 (2014).

High-K toroidal isomers in 28⩽A⩽52

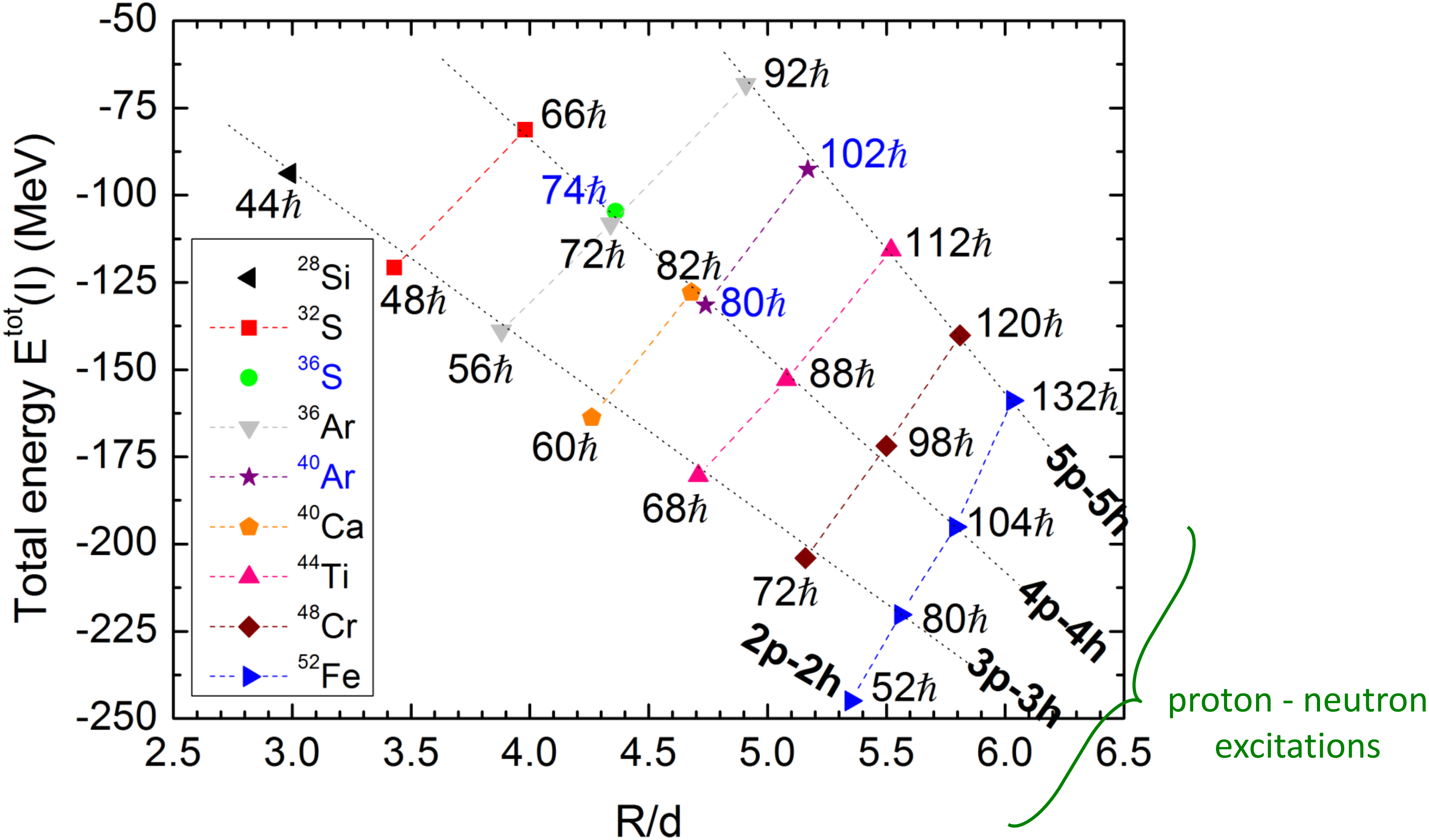

Possible mechanisms for the production of toroidal high-spin isomers (THSI) and toroidal vortex isomers

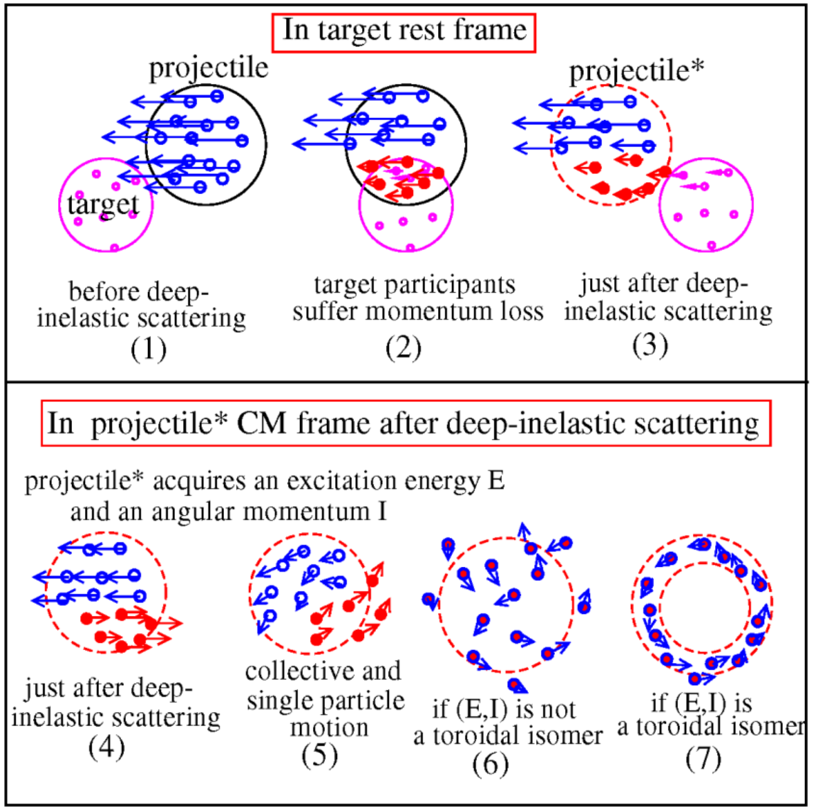

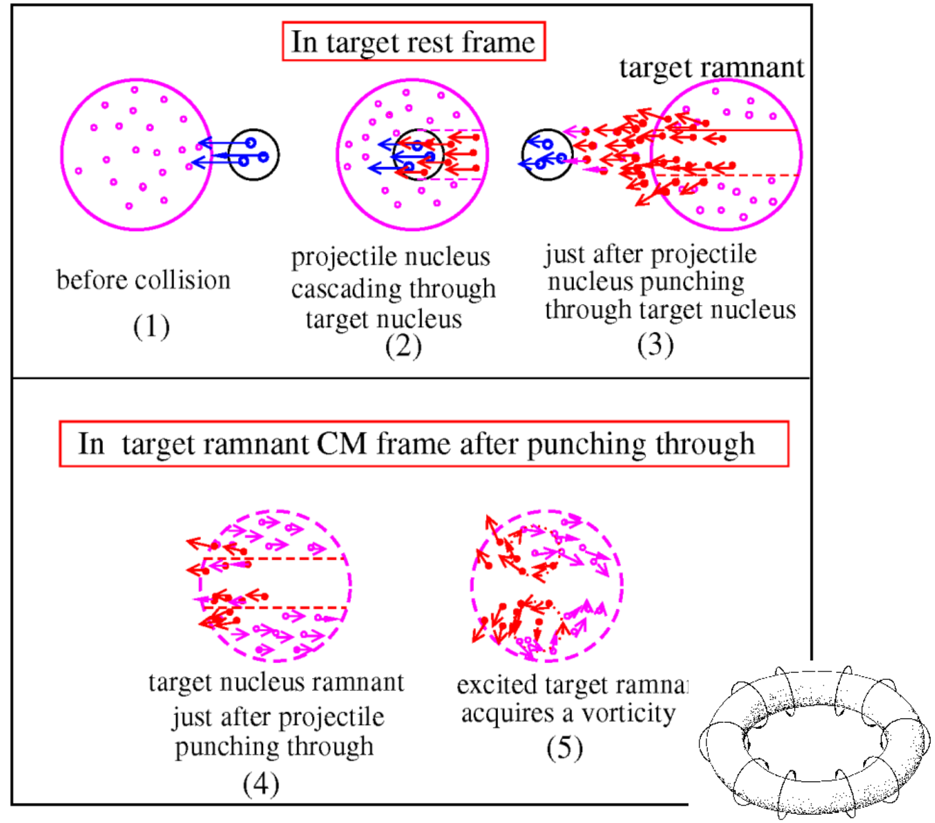

A) Production of a toroidal high-spin isomer by deep-inelastic scattering

B) Production of a toroidal vortex nucleus by punching through a target nucleus

C) Production of light-mass toroidal isomers by elastic scattering – time projection chambers (TPCs) of noble gases under a high voltage

Dziękuję za poświęconą uwagę!

Streszczenie

Badania z wykorzystaniem średnio-polowych modeli samo-zgodnych (z nałożonymi więzami na masowy moment kwadrupolowy Q_{20}) wskazują, że niezależnie od masy jądra atomowego (z liczbą masową $A > 12$) obserwujemy uniwersalny proces ewolucji kształtu jąder. W miarę jak w obliczeniach zmniejsza się zadana wartość momentu kwadrupolowego ($Q_{20} < 0$) elipsoidalne jądro osiąga kształt dysku (deformacja *oblate*), by następnie stać się dyskiem dwustronnie wklęsłym (podobnym do krwinki czerwonej - erytrocytu). Dalsza ewolucja kształtu jądra prowadzi do rozkładu materii jądrowej w postaci torusa.

Należy podkreślić uniwersalny charakter zaobserwowanego zjawiska:
dla dostatecznie dużych wartości deformacji *oblate* "toroidalne rozwiązania" w samo-zgodnych obliczeniach średnio-polowych pojawiają się zarówno dla jąder lekkich jak i najcięższych.

Toroidalne jądro jest układem silnie wzbudzonym i niestabilnym. Okazuje się jednak, że wzbudzenia cząstka-dziura nukleonów, w przypadku takich jąder, prowadzić mogą do izomerycznych (metastabilnych) stanów wysoko-spinowych.

Dodatkowym czynnikiem stabilizującym jądra w kształcie torusa jest liczba atomowa Z. W przypadku, gdy liczba protonów w jądrze osiąga wartość $Z = 132$ (hipotetyczne jądra *hiper-ciężkie*) toroidalne rozwiązania tworzą lokalne płaskie minimum, które wskazuje na możliwość istnienia toroidalnego stanu izomerycznego (bez wzbudzeń cząstka-dziura nukleonów).

Shape transition from a biconcave disc to torus in $^{304}120$

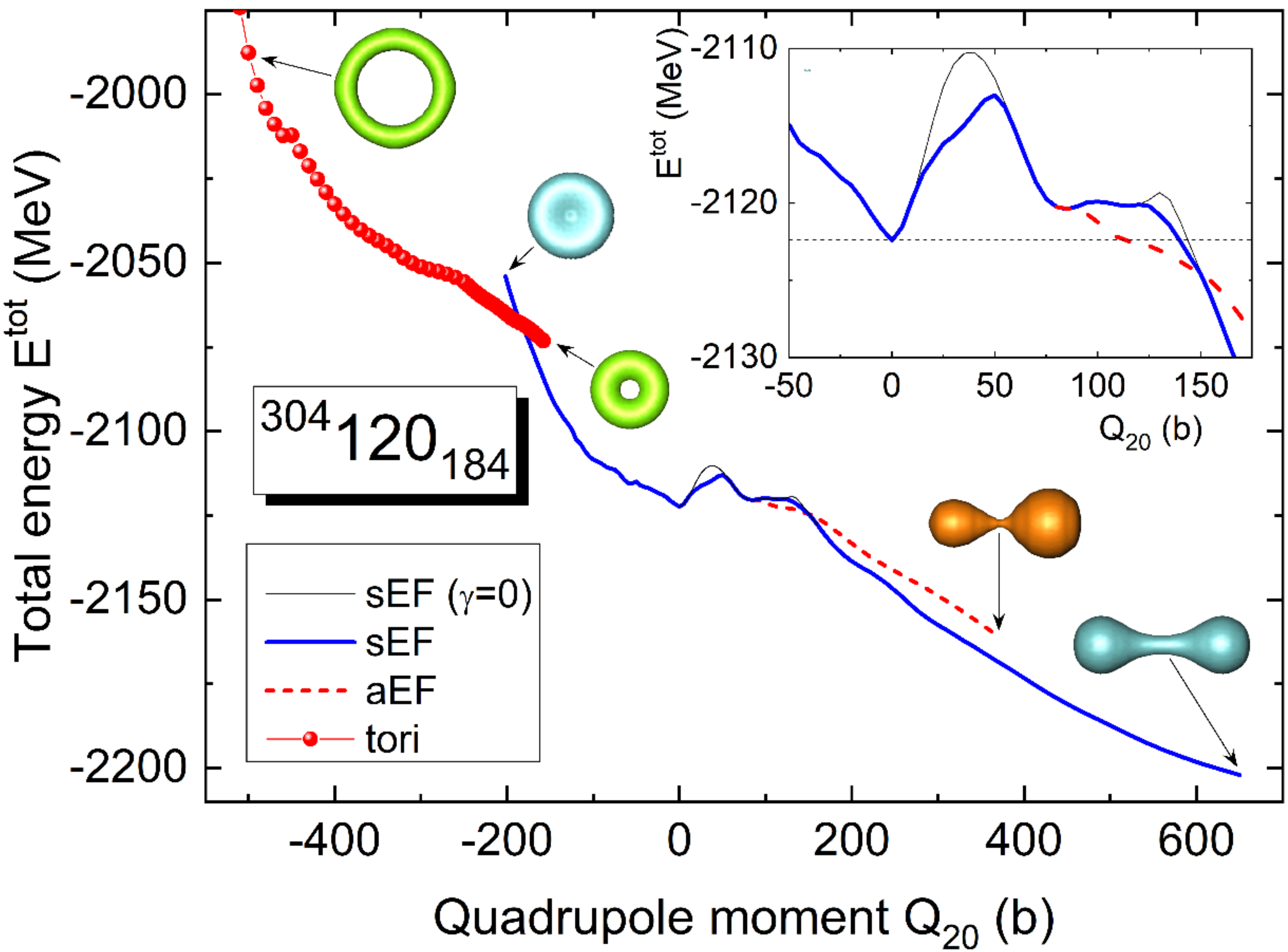

Toroidal high-spin isomers (THSI) in $^{304}120$

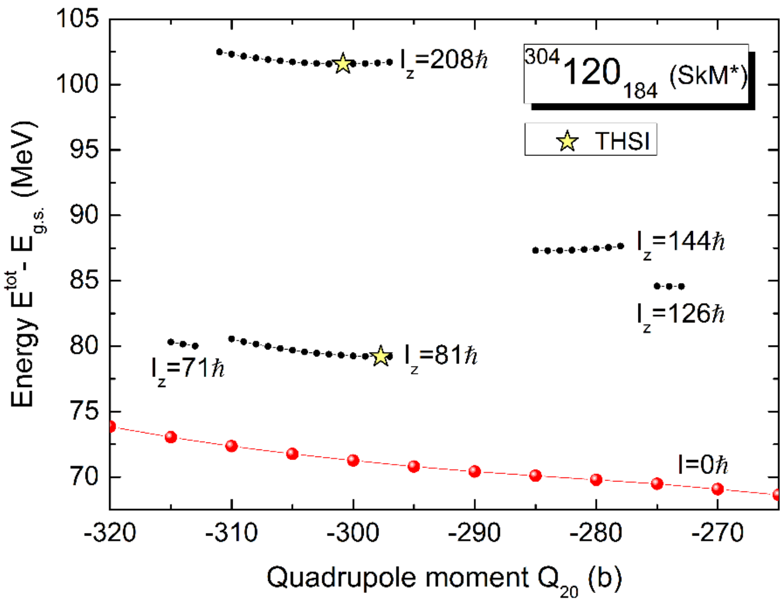

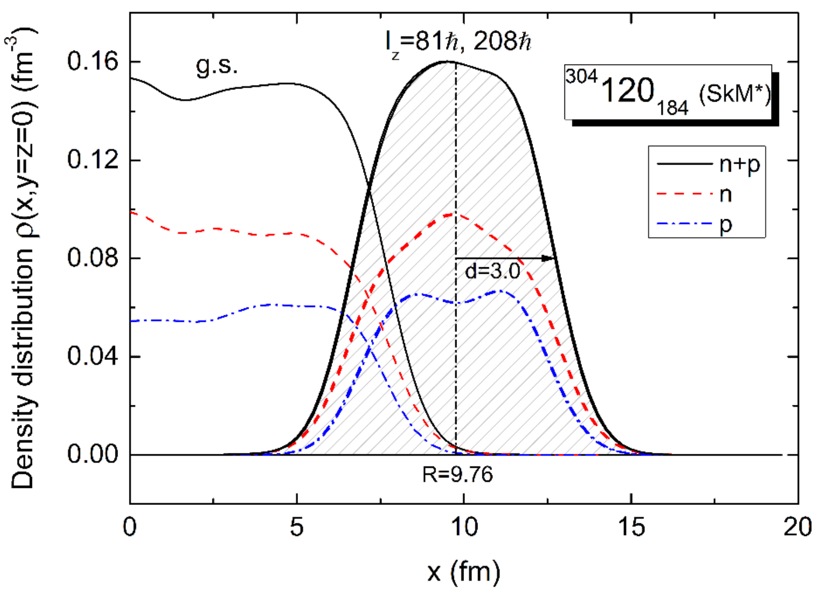

PHYSICAL REVIEW C **95**, 054315 (2017)

TABLE I. The particle-hole excitation configurations leading to the states of $^{304}120_{184}$ with $I_z = I_z(\text{proton}) + I_z(\text{neutron}) = 26 + 55 = 81$ and $I_z = 79 + 129 = 208$.

	Hole states	Particle states
	[11,1,−4] −7/2	[11,0,11] 21/2
$I_z(\text{proton}) = 26$	[12,1,−3] −7/2	[11,1,8] 17/2
	[11,0,−7] −13/2	[12,0,8] 17/2
	[10,1,−7] −13/2	[12,0,12] 25/2
$I_z(\text{proton}) = 79$	[11,0,−11] −23/2	[11,1,8] 15/2
	[10,2,−4] −7/2	[13,0,5] 9/2
	[11,1,−4] −7/2	[13,0,9] 17/2
	[10,1,−9] −17/2	[13,1,6] 13/2
$I_z(\text{neutron}) = 55$	[13,0,−13] −27/2	[10,2,6] 13/2
	[12,0,−12] −23/2	[9,2,5] 11/2
	[13,0,−9] −19/2	[13,1,10] 21/2
	[12,1,−9] −19/2	[14,0,10] 21/2
$I_z(\text{neutron}) = 129$	[10,2,−4] −9/2	[13,0,13] 25/2

Hiper-heavy isotones *N*=196 and isotopes *Z*=132

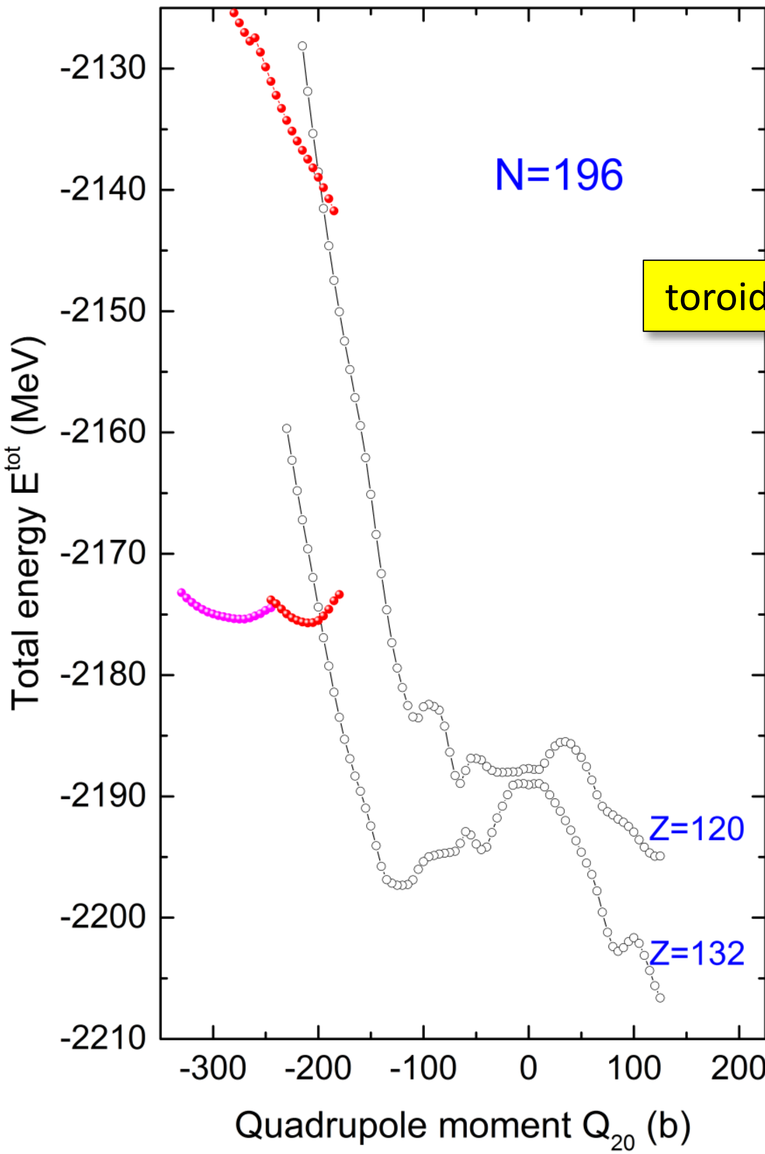

toroidal shape isomers

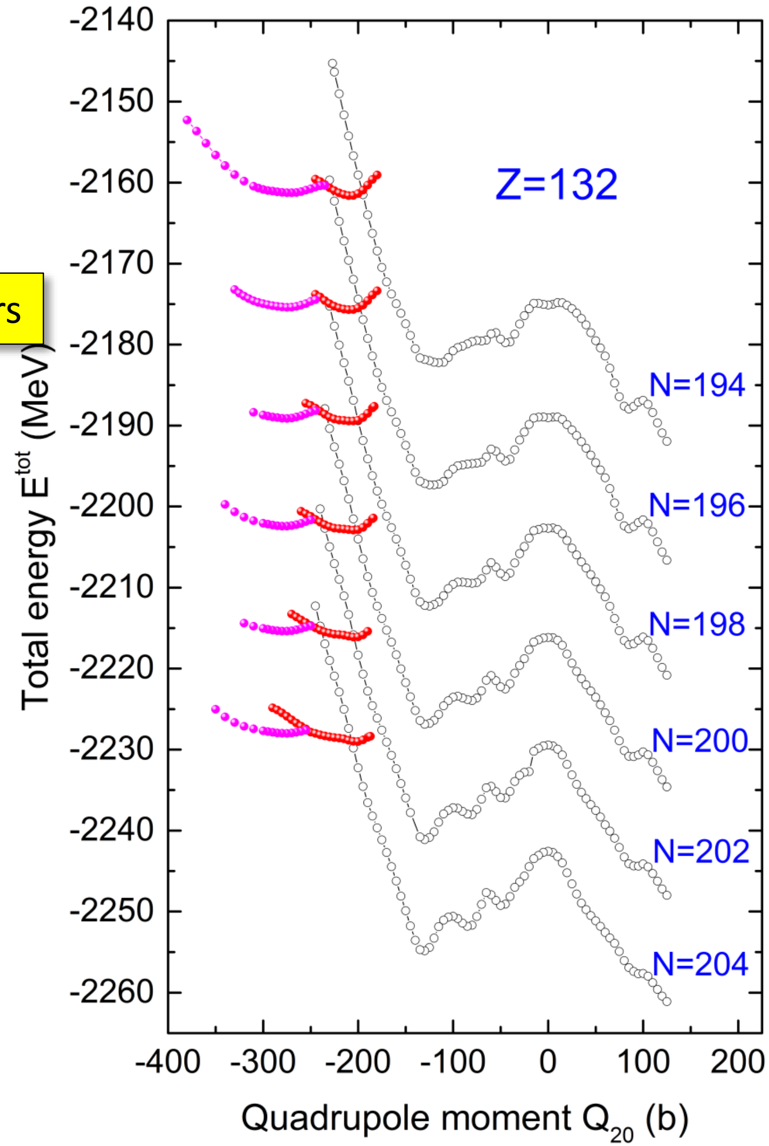

Stability against triaxial distortion

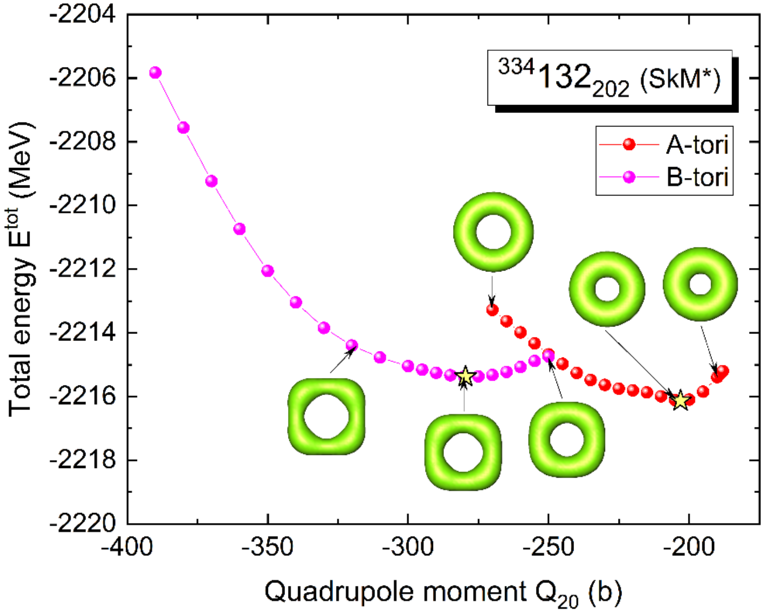

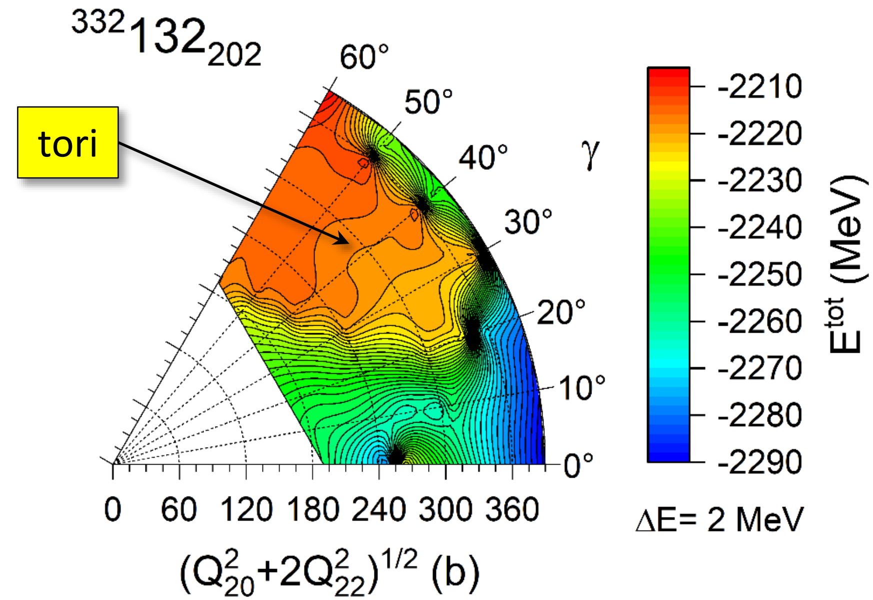

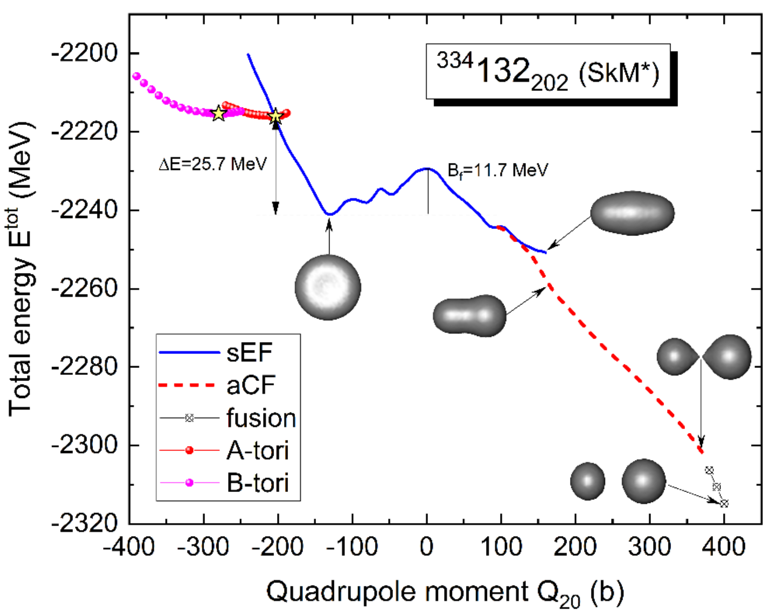

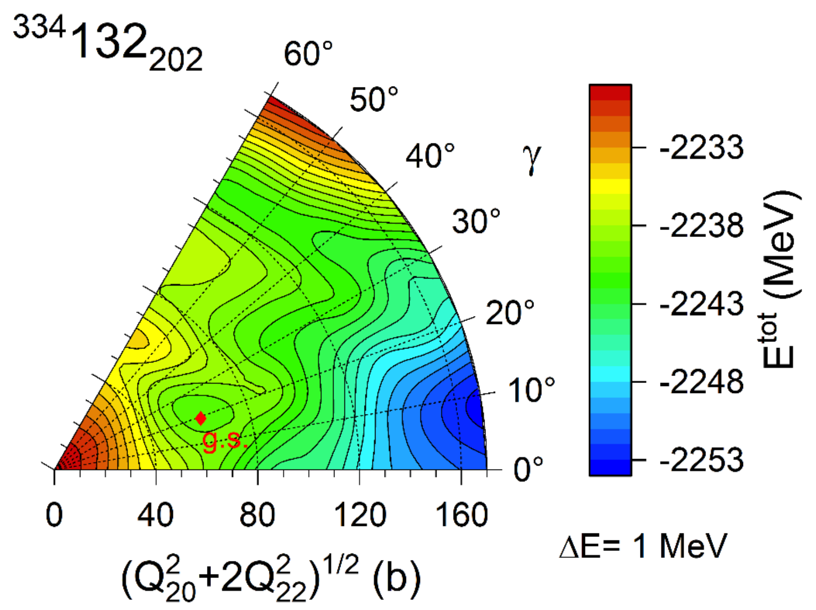

Collaboration

Cheuk-Yin Wong (ORNL), Amelia Kosior (UMCS)

- A. S. and C. Y. Wong, *Toroidal super-heavy nuclei in Skyrme-Hartree-Fock approach*, Acta Phys. Polonica B 40, 1001 (2009).
- A. S. and C. Y. Wong, *A region of high-spin toroidal isomers*, Phys. Lett. B 738, 401 (2014).
- A. S. and C. Y. Wong, *Particle-hole nature of the light high-spin toroidal isomers*, Acta Phys. Polonica B 46, 675 (2015).
- A. S. and C. Y. Wong, *Toroidal high-spin isomers in light nuclei with N≠Z*, Phys. Scr. 90, 114006 (2015).
- A. S. and C. Y. Wong, *Theoretical studies of possible toroidal high-spin isomers in the light-mass region*, EPJ Web of Conferences 117, 04008 (2016).
- A. Kosior, A. S., and C. Y. Wong, *Toroidal nuclear matter distributions of superheavy nuclei from constrained Skyrme-HFB calculations*, Acta Phys. Polonica B Proc. Suppl. 10, 249 (2017).
- A. S., C. Y. Wong, and A. Kosior, *Toroidal high-spin isomers in the nucleus* $^{304}120$, Phys. Rev. C 95, 054315 (2017).
- A. Kosior, A. S., and C. Y. Wong, *Properties of superheavy isotopes Z = 120 and isotones N = 184 within the Skyrme–HFB model*, Acta Phys. Polonica B Proc. Suppl. 11, 167 (2018).
- C. Y. Wong and A. S., *Shells in a toroidal nucleus in the intermediate-mass region*, Phys. Rev. C 98, 034316 (2018).
- X. G. Cao, E. J. Kim, K. Schmidt, K. Hagel, M. Barbui, J. Gauthier, S. Wuenschel, G. Giuliani, M. R. D. Rodriguez, S. Kowalski, H. Zheng, M. Huang, A. Bonasera, R. Wada, N. Blando, G. Q. Zhang, C. Y. Wong, A. Staszczak, Z. X. Ren, Y. K. Wang, S. Q. Zhang, J. Meng, and J. B. Natowitz, *Examination of evidence for resonances at high excitation energy in the 7α disassembly of* ^{28}Si, Phys. Rev. C 99, 014606 (2019).

Toroidal high-K isomers as a possible source of energy?